Mapping Accuracy of Trajectories of Manipulator Motion

Marek Boryga[1], *Paweł* Kołodziej[1*], *Andrzej* Graboś[2], and *Krzysztof* Gołacki[1]

[1] University of Life Sciences in Lublin, ul. Głęboka 28, 20-612 Lublin, Poland
[2] ARKONA, Nasutów 99C, 21-025 Niemce, Poland

Abstract. The paper presents the algorithm for trajectory planning and the analysis of motion accuracy of an anthropomorphic manipulator whose the end-effector moves over the rectilinear-arc path. The path consists of two rectilinear segments of intersecting directions coupled with the arc of a fixed radius. On these rectilinear segments, the end-effector acceleration is described by a polynomial of 7^{th}-degree. The motion over the arc proceeds at a constant velocity. The dynamic analysis was carried out on the basis of Lagrange`s equations of the second order. Manipulator flexibility and damping were considered according to the Kelvin-Voigt model introducing spring-damping components into the drive system. The simulation test results were presented in the form of spatial courses of the pre-assigned and realized trajectories as well as time courses of trajectory end-effector mapping errors for three paths with different radii of the arc.

1 Introduction

One of the fundamental tasks in trajectory planning operation proves to be the analysis of errors resulting from the manipulator dynamic chain deformability. Manipulator structure, geometry, mass distribution as well as its shape and position in the task space of the desired path have, besides the stiffness and damping, a significant effect on the mappability of the prescribed trajectory. Erkorkmaz et al. [5] proposed a trajectory planning strategy for maintaining the tool positioning accuracy in high speed cornering applications. A 3D contour error estimation algorithm was presented for determining the geometric deviation from the arbitrarily shaped toolpaths. Two spline fitting strategies were developed for smoothening sharp corners. Dong et al. [4] examined the possibility of scheduling or varying the feed-rate by taking into consideration the geometry of the contour that the machine is expected to follow and the physical capabilities of the machine. The paper presents, the constraints on permissible jerk and as a consequence, machine vibrations got reduced, element wear declined and mapping errors in the end-effector path limited. Tseng et al. [8] suggested an algorithm for the jerk-limited acceleration planning. With this algorithm, both the chord error, the maximum acceleration and jerk were within the permissible limits.

Apart from the factors mentioned at the beginning, which influence the accuracy of movement, the way of trajectory parameterization is also very important. Among the

* Corresponding author: pawel.kolodziej@up.lublin.pl

applied methods, parameterization with the use of higher degree polynomials is worthy of mention. Thus way it is possible to obtain smooth trajectories with simultaneous limitation of speed, acceleration or jerk. Boryga and Graboś [1] used polynomials of higher degree for trajectory planning of robot manipulator. The linear acceleration profiles of end-effector were planned as the polynomials of 9, 7 and 5 degree. They also demonstrated the algorithm for Polynomial Cross Method (PCM) to plan the end-effector motion whose path is composed of two rectilinear segments [6]. Boryga et al. [2] applied the Planning Rectilinear-Arc Polynomial Trajectory (PR-APT) method for planning the end-effector motion trajectory during harvesting tomatoes in the greenhouse. The acceleration profile of end-effector was planned as the polynomial of 7^{th}-degree. Milica et al. [7] presented the method for determining the optimal trajectory of a parallel robot. The Hermite polynomial expressions were used as the time function of geometrical parameters. The authors concluded that the use of polynomial functions with the simplest expressions leads to minimization of effort associated with the analysis and mathematical formulation of the optimization problem. Chen et al. [3] proposed the Intermediate Point Obstacle Avoidance (IPOA) algorithm to provide smooth trajectory and efficient movement while avoiding obstacles. Combining the IPOA algorithm in a series, multi-obstacle avoidance by the robotic arm in the complex environment can be accomplished.

The paper is arranged as follows. Chapter II proposes an innovative and very effective algorithm for planning rectilinear-arc trajectories of manipulator end-effector. On the rectilinear segments the acceleration course is described by the polynomial of 7^{th}-degree. Transition from the rectilinear segment to the arc and vice versa proceeds without a change of velocity. Chapter III presents the dynamics model. Flexibility and damping forces in kinematic pairs were taken into consideration introducing spring-damping components into the drive system. Chapter IV depicts the numerical example. For the planned rectilinear-arc trajectory (for three arc radii), prescribed and realized trajectories of end-effector and time courses of position errors were presented.

2 Planning of rectilinear-arc trajectories of end-effector motion

1.1 Assumptions

The first stage in planning a rectilinear-arc trajectory is as follows:

- Coordinates of the initial B, final E and intermediate M points. The points B and E should be located in the workspace of the robot manipulator. The point M is the intersection point of the rectilinear segments and does not lie on the planned path. It can be situated outside the workspace (Fig.1).
- Arc radius R.
- Maximum acceleration on the rectilinear segments a_{max}.

1.2 Algorithm for trajectory planning

Step 1. Determine the scalar equation of the plane π passing through the points B, M, and E.

Step 2. Define the parametric equations of the straight line passing through the points B and M as well as points E and M.

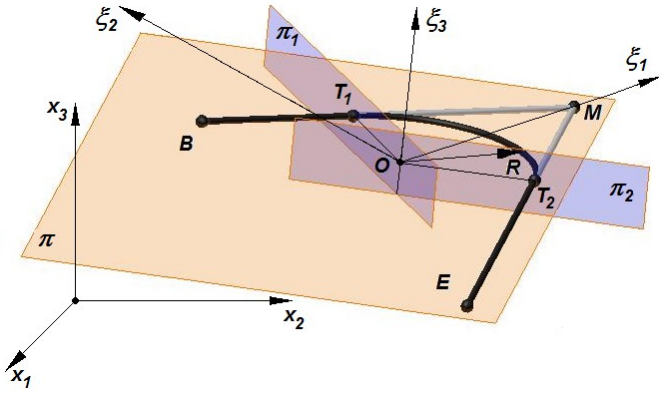

Fig. 1. The rectilinear-arc motion path with the added coordinate systems

Step 3. Establish equations of the π_1 and π_2 planes perpendicular to the straight lines passing through the points B and M (π_1 planes) as well as the points E and M (π_2 planes) and those passing through the center of the arc O.

Step 4. Determine the coordinates of point T_1 as common to the plane π_1 and the straight line running through the points B and M as well as the coordinates of the point T_2 as the common to the plane π_2 and the straight line passing through the points E and M.

Step 5. Define the coordinates of the center of the arc O that lies in the plane π and is tangential to the points T_1 and T_2 to the segments BM and ME.

Step 6. Determine the apex BME and the apex T_1OT_2 angles.

Step 7. Determine matrix transformation $\boldsymbol{A}$ between the local system of coordinates $\xi_1\xi_2\xi_3$ connected with arc and the reference coordinate system $x_1x_2x_3$. The origin of the system $\xi_1\xi_2\xi_3$ is the point O, versor of ξ_1 axis oriented towards the point M and the direction of ξ_2 axis versor intersecting the line passing through the points B and M. The versor of ξ_3 axis is a complement of the right-handed coordinate system.

Step 8. Determine path increments on the rectilinear segments Δs^{BT1} and Δs^{T2E}.

Step 9. Pre-establish motion time for the BT_1 and T_2E segments

$$t = \frac{3\sqrt{210}\sqrt[4]{21}\sqrt{\Delta s \cdot a_{max}}}{49 a_{max}} \tag{1}$$

For the segment BT_1: $t=t^{BT1}$, $\Delta s=\Delta s^{BT1}$. For the segment T_2E: $t=t^{T2E}$, $\Delta s=\Delta s^{T2E}$.

Step 10. Determine velocity in the T_1 and T_2 tangency points

$$v = \frac{105}{64}\frac{\Delta s}{t} \tag{2}$$

For the segment BT_1: $v=v_{T1}$, $\Delta s=\Delta s^{BT1}$ and $t=t^{BT1}$. For the segment T_2E: $v=v_{T2}$, $\Delta s=\Delta s^{T2E}$ and $t=t^{T2E}$.

Step 11. Determine motion time on the BT_1 and T_2E segment.

If $v_{T1}\geq v_{T2}$, then velocity in the tangency points and over the arc should be assumed to be $v^{Arc}=v_{T2}$ and the motion time on the BT_1 segment is derived from the dependency (2) where $t=t^{BT1}$, $\Delta s=\Delta s^{BT1}$ and $v=v_{T2}$ should be substituted. In the case $v_{T1}<v_{T2}$, the velocity at the tangential points and on the arc should be assumed to be $v^{Arc}=v_{T1}$ while the motion time on T_2E segment is derived from the dependency (2) where $t=t^{T2E}$, $\Delta s=\Delta s^{T2E}$ and $v=v_{T1}$ should be substituted.

Step 12. Establish the polynomial coefficient for calculation of acceleration, speed and position for the BT_1 and T_2E segments

$$p = \frac{315}{8}\frac{\Delta s}{t^9} \tag{3}$$

For the segment BT_1: $p=p^{BT1}$, $\Delta s=\Delta s^{BT1}$ and $t=t^{BT1}$. For the segment T_2E: $p=p^{T2E}$, $\Delta s=\Delta s^{T2E}$ and $t=t^{T2E}$.

Step 13. Determine the motion duration time over the arc

$$t^{Arc} = \frac{\beta \cdot R}{v^{Arc}} \tag{4}$$

Step 14. Define the dependence on angular displacement in motion over the arc

$$\beta(t) = \frac{\beta}{2} - \frac{v^{Arc}}{R}(t - t^{BT1}) \text{ for } t^{BT1} \le t \le t^{BT1} + t^{Arc} \tag{5}$$

Step 15. Determine the coordinates of the vectors of position $\boldsymbol{X}^{Arc}$, speed $\boldsymbol{X'}^{Arc}$ and acceleration $\boldsymbol{X''}^{Arc}$ of the motion over the arc in the coordinate system $x_1x_2x_3$

$$\boldsymbol{X}^{Arc} = \boldsymbol{A} \cdot \boldsymbol{\Xi}^{Arc},\ \boldsymbol{X'}^{Arc} = \boldsymbol{A} \cdot \boldsymbol{\Xi'}^{Arc},\ \boldsymbol{X''}^{Arc} = \boldsymbol{A} \cdot \boldsymbol{\Xi''}^{Arc} \tag{6}$$

where: $\boldsymbol{X}^{Arc}=[x_1^{Arc}(t), x_2^{Arc}(t), x_3^{Arc}(t), 1]^T$, $\boldsymbol{\Xi}^{Arc}=[R\cos\beta(t), R\sin\beta(t), 0, 1]^T$

Step 16. Determine translation in time on the T_2E segment

$$t_b = t^{BT1} - t^{T2E} + t^{Arc} \tag{7}$$

Step 17. Perform translation in time of the polynomial depicting the acceleration profile for the T_2E segment by tb value

$$a^{BT1}(t) = -p^{BT1} \cdot (t)^2 \cdot (t - t^{BT1})^3 \cdot (t - 2t^{BT1})^2 \tag{8}$$

$$a^{T2E}(t) = p^{T2E} \cdot (t - t_b)^2 \cdot (t - t^{T2E} - t_b)^3 \cdot (t - 2t^{T2E} - t_b)^2 \tag{9}$$

Step 18. Set the total motion time on the designated trajectory

$$t_{end} = t^{BT1} + t^{Arc} + t^{T2E} \tag{10}$$

3 Dynamics of the open kinematic chain

The motion equations were derived on the basis of the Lagrange equations of the second order. The general form of the equations is written as follows

$$\boldsymbol{B}(\theta)\boldsymbol{\theta''} + \boldsymbol{O}(\theta)\boldsymbol{\theta'}^2 + \boldsymbol{C}(\theta)\boldsymbol{\theta'}\boldsymbol{\theta'} + \boldsymbol{G}(\theta) = \boldsymbol{\tau} \tag{11}$$

where: $\boldsymbol{B}(\theta)$ - the inertia matrix, $\boldsymbol{O}(\theta)$ - the matrix of centrifugal torques, $\boldsymbol{C}(\theta)$ - the matrix of Coriolis torques, $\boldsymbol{G}(\theta)$ - the vector of gravity torques, $\boldsymbol{\tau}$ - the generalized joint force vector.

The dynamics model takes into account flexibility and damping effects introducing deformable objects (Kelvin-Voigt model) between the drive units and links. The forces generalized in *i*-nth kinematic pair were defined by the equation

$$\tau_i = k_{si}(\theta_{gi} - \theta_{ri}) + c_{di}(\theta'_{gi} - \theta'_{ri}) \tag{12}$$

where: k_{si} - the stiffness coefficient [Nm/rad], c_{di} - the viscous damping coefficient [Nms/rad], θ_{gi} - the prescribed link *i* angular displacement [rad] and θ_{ri} - the accomplished link *i* angular displacement [rad].

4 Numerical example

The simulation tests were performed for three degrees of freedom anthropomorphic manipulator (Fig.2). Geometrical and mass values are presented in Table 1.

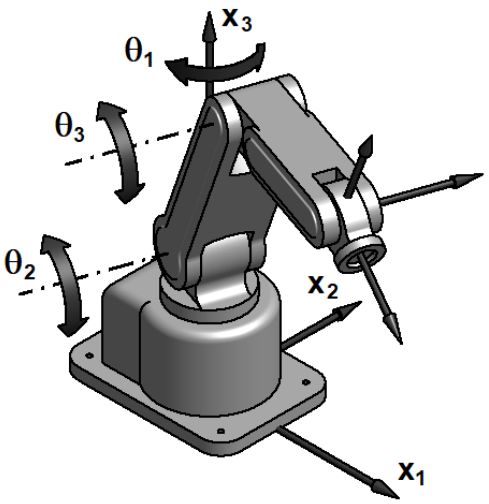

Fig. 2. The anthropomorphic manipulator

Table 1. The geometrical and mass values of manipulator

Link number	Length [m]		Mass [kg]		Mass inertial moment [kgm^2]					
1	λ_1	0.85	m_1	26.2	I_{x1}	–	I_{y1}	0.92	I_{z1}	–
2	l_2	0.95	m_2	10.2	I_{x2}	0	I_{y2}	1.5	I_{z2}	1.5
3	l_3	0.65	m_3	7.2	I_{x3}	0	I_{y3}	0.68	I_{z3}	0.68

The same value for the stiffness coefficient was assumed for all the links, i.e. k_s =2500 Nm/rad and for the viscous damping coefficient c_d =250 Nms/rad. The coordinates of *B*, *E* and *M* points are *B*(0.5,0.5,1), *E*(0.75,0.75,1), *M*(0.5,0.75,1). The assumed maximum acceleration was a_{max} =0.25m/s^2. The simulation tests were conducted for three paths with the arc radii equal to: R_1=0.025m (*Path* 1), R_2=0.01m (*Path* 2) and R_3=0.005m (*Path* 3). The coordinates of the characteristic points of trajectory are presented in Table 2.

Table 2. The coordinates of characteristic points of paths

Path	Tangent point T_1			Tangent point T_2			Arc center O		
	x_1^{T1}	x_2^{T1}	x_3^{T1}	x_1^{T2}	x_2^{T2}	x_3^{T2}	x_1^{O}	x_2^{O}	x_3^{O}
Path 1	0.5	0.725	1	0.525	0.75	1	0.525	0.725	1
Path 2	0.5	0.74	1	0.51	0.75	1	0.51	0.74	1
Path 3	0.5	0.745	1	0.505	0.75	1	0.505	0.745	1

In order to determine the pre-assigned angular displacements at each kinematic pair θ_{g1}, θ_{g2}, θ_{g3} the inverse kinematics problem was solved. There were established the accomplished angular displacements θ_{r1}, θ_{r2}, θ_{r3} as a result of numerical integration of the motion equations (11) and the end-effector positions x_{r1}, x_{r2}, x_{r3} on the basis of the simple problem of kinematics. The end-effector position errors Δx_i were calculated from the dependence $\Delta x_i = x_{gi} - x_{ri}$ for i = 1, 2, 3. The simulation experiments provided the courses of the pre-assigned and accomplished trajectory of end-effector motion and the time courses of end-effector position errors (Fig.3).

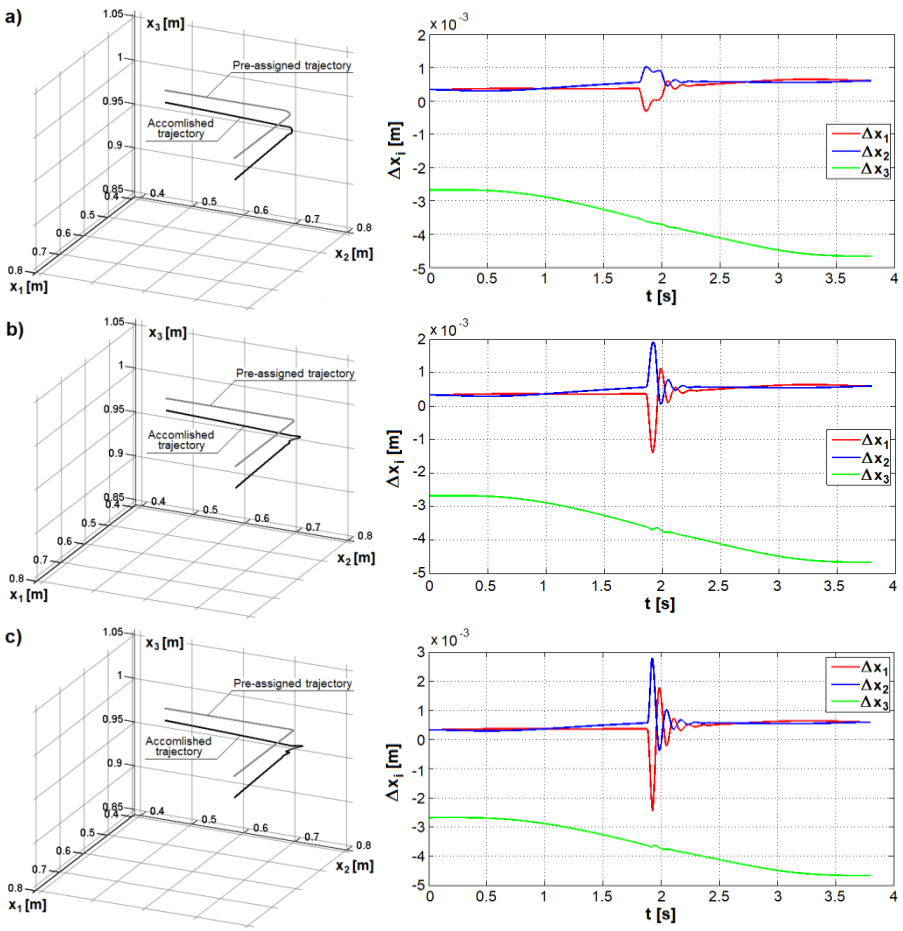

Fig. 3. The pre-assigned and accomplished end-effector trajectory (position error at 5-fold magnification) and the end-effector position errors for: a) *Path* 1, b) *Path* 2, c) *Path* 3

The polynomial coefficients, motion times and motion velocities over the arcs are presented in Table 3.

Table 3. The characteristic values of the planned trajectories

Path	$p^{BT1} = p^{T2E}$ [m/s^9]	$t^{BT1} = t^{T2E}$ [s]	v^{Arc} [m/s]	t^{Arc} [s]	t_{end} [s]
Path 1	0.044401	1.802	0.205	0.192	3.795
Path 2	0.035311	1.861	0.212	0.074	3.796
Path 3	0.032852	1.880	0.214	0.037	3.797

The maximum absolute mapping errors of trajectory are presented in Table 4.

Table 4. The maximum absolute mapping errors of trajectory

Trajectory mapping error	Path denotation		
	Path 1	*Path* 2	*Path* 3
Δx_1 [m]	$6.41 \cdot 10^{-4}$	$1.39 \cdot 10^{-3}$	$2.44 \cdot 10^{-3}$
Δx_2 [m]	$1.02 \cdot 10^{-3}$	$1.92 \cdot 10^{-3}$	$2.79 \cdot 10^{-3}$
Δx_3 [m]	$4.67 \cdot 10^{-3}$	$4.67 \cdot 10^{-3}$	$4.67 \cdot 10^{-3}$

5 Conclusions

Based on the analysis using the proposed algorithm for planning of rectilinear-arc trajectories of the end-effector there can be drawn, the following conclusions:

- The arc radius was found to have a minor effect on the total motion time and at the same time significant influence on position errors. The change of the arc radius from R_1=0.025m (*Path* 1) to R_2=0.01m (*Path* 2) results in the about 2-fold increase in the trajectory mapping errors toward x_1 and x_2 while from R_1=0.025m (*Path* 1) to R_3=0.005m (*Path* 3) – an approximately 4-fold increase. Motion time growth was equal to 0.001s and 0.002s, respectively.
- The errors on the x_1 and x_2 directions result from dynamic loads as the pre-assigned motion proceeded in the x_1x_2 plane. The error toward the x_3 axis is mainly associated with the static load and proved to be almost the same for each arc radius.
- Owing to the assumed small linear acceleration, the dynamic load errors (inertia, centrifugal and Coriolis forces) are smaller than those caused by the static load.
- The errors toward the x_3 axis result from the angular position errors of the second and third links whereas those toward the x_1 and x_2 axes arise chiefly from the angular position error of the first link.

References

1. M. Boryga, A. Graboś, Mech. Mach. Theory **44**, 1400-1419 (2009)
2. M. Boryga, A. Graboś, P. Kołodziej, K. Gołacki, Z. Stropek, Agriculture and Agricultural Science Procedia, **7**, 27-34 (2015)
3. Z. Chen, W.H. Su, B. Li, B.S. Deng, H. Wu, B.Z. Liu, Adv. Mech. Eng. **10**, 1-15 (2018)
4. J. Dong, P.M. Ferreira, J.A. Stori, Int. J. Mach. Tool. Manu. **47**, 1941-1955 (2007)
5. K. Erkorkmaz, C.H. Yeung, Y. Altintas, Int. J. Mach. Tool. Manu. **46**, 1124-1138 (2006)
6. A. Graboś, M. Boryga, Eksploat. Niezawodn. **15**, 182-187 (2013)
7. L. Milica, A. Năstase, G. Andrei, Mech. Mach. Theory **128**, 14-33 (2018)
8. S.J. Tseng, K.Y. Lin, J.Y. Lai, W.D. Ueng, J. Chin. Inst. Eng. **32**, 215-228 (2009)